# A spatially restricted increase in receptor mobility is involved in directional sensing during *Dictyostelium discoideum* chemotaxis

**Sandra de Keijzer[1,2], Arnauld Sergé[1], Freek van Hemert[1], Piet H. M. Lommerse[1,2], Gerda E. M. Lamers[2], Herman P. Spaink[2], Thomas Schmidt[1,*] and B. Ewa Snaar-Jagalska[2,*]**

[1]Physics of Life Processes, Leiden Institute of Physics, Leiden University, Niels Bohrweg 2, 2333 CA Leiden, The Netherlands
[2]Cell Biology, Leiden Institute of Biology, Leiden University, PO Box 9504, 2300 RA Leiden, The Netherlands
*Authors for correspondence (e-mails: schmidt@physics.leidenuniv.nl; b.e.snaar-jagalska@biology.leidenuniv.nl)

*Accepted 25 February 2008*
*Journal of Cell Science 121, 1750-1757 Published by The Company of Biologists 2008*
*doi:10.1242/jcs.030692*

## Summary

**The directed cell migration towards a chemotactic source, chemotaxis, involves three complex and interrelated processes: directional sensing, cell polarization and motility. Directional sensing allows migrating eukaryotic cells to chemotax in extremely shallow gradients (<2% across the cell body) of the chemoattractant. Although directional sensing has been observed as spatially restricted responses along the plasma membrane, our understanding of the 'compass' of the cell that controls the gradient-induced translocation of proteins during chemotactic movements is still largely lacking. Until now, the dynamical behaviour and mobility of the chemoattractant-receptor molecule has been neglected in models describing the directional sensing mechanisms. Here, we show by single-molecule microscopy an agonist-induced increase in the mobile fraction of cAMP-receptor at the leading edge of chemotacting *Dictyostelium discoideum* cells. The onset of receptor mobility was correlated to the uncoupling and activation of the Gα2-protein. A finite-element simulation showed that the increase in mobile fraction of the activated receptor enabled the amplified generation of activated Gβγ-dimers at the leading edge of the cell, faithfully representing a primary linear amplification step in directional sensing. We propose here that modulation of the receptor mobility is directly involved in directional sensing and provides a new mechanistic basis for the primary amplification step in current theoretical models that describe directional sensing.**

Supplementary material available online at
http://jcs.biologists.org/cgi/content/full/121/10/1750/DC1

Key words: Single-molecule microscopy, Chemotaxis, *Dictyostelium discoideum*, G-protein-coupled receptor

## Introduction

Most eukaryotic cells chemotax by converting shallow differences of extracellular chemoattractant gradient into highly localized intracellular responses (Affolter and Weijer, 2005; Parent et al., 1998). Directional sensing is the ability of the cell to determine the direction of extracellular cues and can be thought of as a 'compass' (Franca-Koh et al., 2006). The local accumulation of PtdIns(3,4,5)$P_3$ at the leading edge of chemotacting cells as a result of the reciprocal localization of the phosphatidylinositol 3-kinase (PI3K) and the PI3 phosphatase (PTEN) has been proposed to act as the internal compass (Weiner, 2002). However, recent evidence in the amoebae *Dictyostelium discoideum* shows that a mutant lacking all PI3K and the PTEN phosphatase is still able to sense direction (Hoeller and Kay, 2007). Another study in which the function of the six PI3Ks in *D. discoideum* was characterized suggests that other signalling pathways are possibly sufficient in directional sensing in response to a high signal, but that PI3K signalling is crucial for detecting weak signals (Takeda et al., 2007). Indeed, recently, another pathway was found in *D. discoideum*, involving the phospholipase A2, that acts in parallel to the PI3K pathway (Chen et al., 2007). As the signalling network is branched into these parallel pathways after G-protein-coupled receptor (GPCR)-mediated activation of a G protein, and the GPCR and G-protein are the only crucial components of the pathway, one might expect the compass of the cell to be at this level of the signalling pathway.

Until now, this idea has been rejected because the cAR1-receptor and the Gα2/βγ proteins, remain uniformly distributed along the cell surface, as demonstrated using fluorescent cAR1 and Gβ subunit in *D. discoideum* (Jin et al., 2000; Xiao et al., 1997). FRET studies between the G-protein subunits revealed a higher GPCR-mediated activation of the G-proteins at the leading edge (Xu et al., 2005). However, this was interpreted as directly reflecting the receptor occupancy. Owing to technical difficulties, the GPCR activation of the G-protein has never been directly visualized, although the dynamics of activation is of the highest importance when interpreting the FRET data correctly. It has been found using single-molecule microscopy of fluorescence-labelled cAMP, that the dissociation rate of cAMP at the leading edge of the cell was twice that at the trailing edge (Ueda et al., 2001). It is therefore tempting to speculate that directional sensing is directly related to the acceleration of the activation step of the G-protein-linked signalling pathways at the leading edge. This theory is addressed here by exploring whether the mobility of the receptor exhibits an asymmetry, which in turn could account for the primary decision in the spatially restricted response of the downstream signalling pathway during cell migration.

## Results

In order to analyze the mobility of the receptor in detail, it was necessary to monitor individual fluorescent receptors. Therefore, the cAMP receptor cAR1 of *D. discoideum* was fused to eYFP and stably expressed in receptor-deficient *car1*$^-$ cells to an expression level that resembles that of the endogenous receptor in wild-type cells (see Fig. 1A, and Materials and Methods). The fusion protein proved to be effectively synthesized and targeted to the plasma membrane (Fig. 1B). The molecular weight and stability of the fusion protein was validated by immunoblot of whole-cell extracts of transformed *car1*$^-$ cells using a purified GFP antibody. As shown in Fig. 1A, the receptors appeared as a single band at the predicted size of ~70 kDa. cAR1-eYFP was functionally indistinguishable from wild-type cAR1, as the fusion protein complemented the deficiency of the cAR1 protein and completely rescued the developmental program (Devreotes, 1994) of *car1*$^-$ cells, including the aggregation process and the formation of a fruiting body (Fig. 1C, bottom right). By contrast, *car1*$^-$ cells could not undergo development beyond the one-cell state (Fig. 1C, top left).

Single-molecule microscopy (SMM), a combination of regular wide-field microscopy with laser excitation and ultra-sensitive CCD camera detection, was used to obtain high spatial (~40 nm) and temporal (~44 mseconds) resolution information on the mobility of cAR1 receptors. In order to reach a density of fluorescent receptors at which individual molecules could be observed (<1/μm$^2$), cells were photobleached prior to imaging (Fig. 1D). As photobleaching occurs at random, we assume that the unbleached population of receptors is a fully representative subpopulation of all receptors. As predicted for individual molecules, fluorescence signals were characterized by diffraction-limited spots on the camera that exhibited single-step photobleaching typical for single molecules (Fig. 1E). This finding was independent of position, stage of cellular development, mutations or stimulation protocol. Images were taken at a rate of 23 frames/second. Automated analysis yielded values for the integrated fluorescence signal and the lateral position of the receptors (accuracy ~40 nm) (Schmidt et al., 1996). From the receptor positions in consecutive images, trajectories of individual cAR1-eYFP were reconstructed (Fig. 1F).

Trajectories of cAR1-eYFP similar to that shown in Fig. 1F from the top membrane of control cells were further analyzed to study the receptor mobility. For the analysis, the cumulative probability (P) of the squared displacements ($r^2$, see Materials and Methods) was determined (Schutz et al., 1997) for a time delay between images set to 44 mseconds (Fig. 2). Two-thousand-and-sixty trajectories were analyzed, and squared displacements up to 0.2 μm$^2$ were found. Fig. 2A shows the data for a control cell that followed the developmental cycle for 2-3 hours (see Materials and Methods), at which point Gα2 proteins were expressed (Kumagai et al., 1989) but no endogeneous cAMP was detected (Kesbeke et al., 1986). It should be noted that Gβγ proteins were constitutively present in the plasma membrane of *D. discoideum*. Subsequently, cells were brought to an early aggregation stage by starvation during which they are gradient-sensing competent (Fig. 2B). This procedure is referred to in the following as natural assay. The leading and trailing edge of each cell was defined with respect to the centre of the aggregate. The cumulative probability distributions of the squared displacements of receptors located at the anterior and posterior of chemotaxing cells, respectively, showed a slight difference (Fig. 2B). In order to quantify the significance of that difference, we applied a statistical two-sample Kolmogorov-Smirnov test (KS-test)

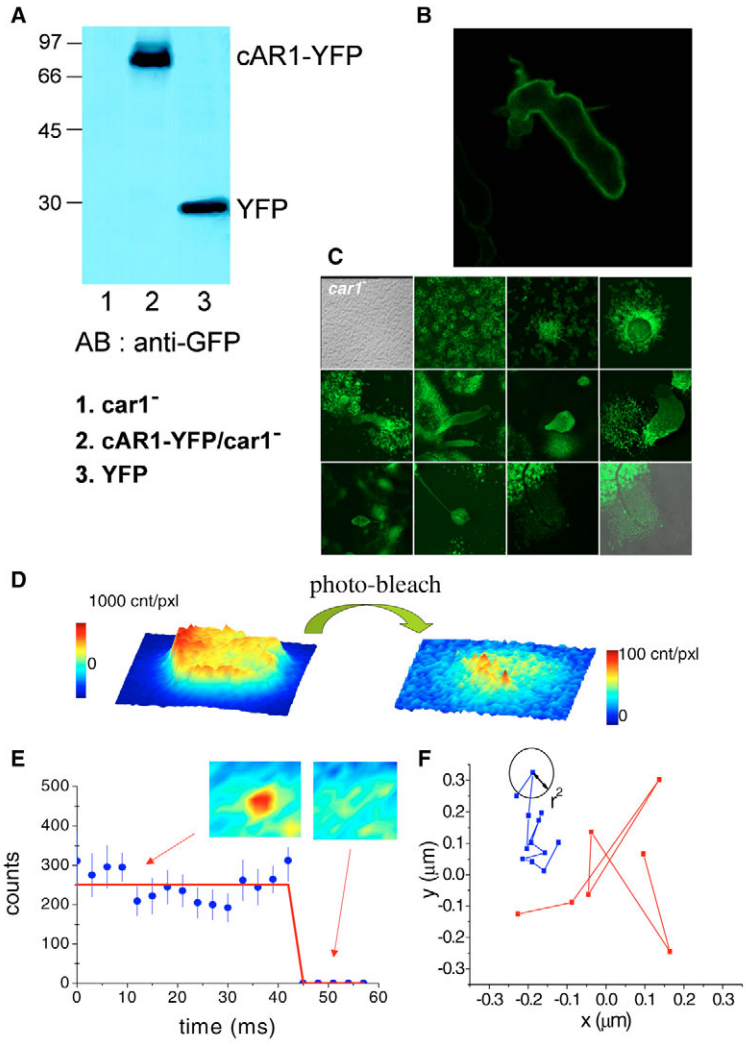


**Fig. 1.** Generation of cell lines expressing cAMP-receptor/eYFP fusion proteins at endogenous levels. (A) Detection of cAR1-eYFP fusion protein by western blot using an anti-GFP antibody. Free YFP showed the expected band at ~30 kDa (lane 3). As cAR1 has a size of 40 kDa, the correct size for the fusion protein is 70 kDa, which was observed (lane 2). Transformed *car1*$^-$ cells with the cAR1-eYFP fusion protein exhibited a protein-band at the correct size (lane 2), whereas *car1*$^-$ cells did not (lane 1). Free eYFP was not detected in cAR1-eYFP/ *car1*$^-$ cells. (B) cAR1-eYFP was localized at the plasma membrane of *car1*$^-$ cells, as detected by confocal microscopy. (C) The first image shows the aggregation-deficient phenotype of *car1*$^-$ mutant 24 hours after starvation. These cells were not able to initiate the developmental cycle. The following images display the different developmental stages of *car1*$^-$ cells transformed with the cAR1-eYFP construct. The developmental defect of *car1*$^-$ cells was rescued by the cAR1-eYFP transformation. (D) The left picture shows a fluorescence image of the top membrane of a typical unstimulated *car1*$^-$ cell transformed with cAR1-eYFP. After a brief photobleaching pulse (2.5-5.0 seconds) individual receptors were detected (peaks of fluorescence in the right image). (E) Fluorescence signal of an individual cAR1-eYFP molecule as a function of time, showing a single-step photobleaching event characteristic for individual molecules. (F) Two examples of trajectories of individual cAR1-eYFP molecules diffusing in the top plasma membrane.

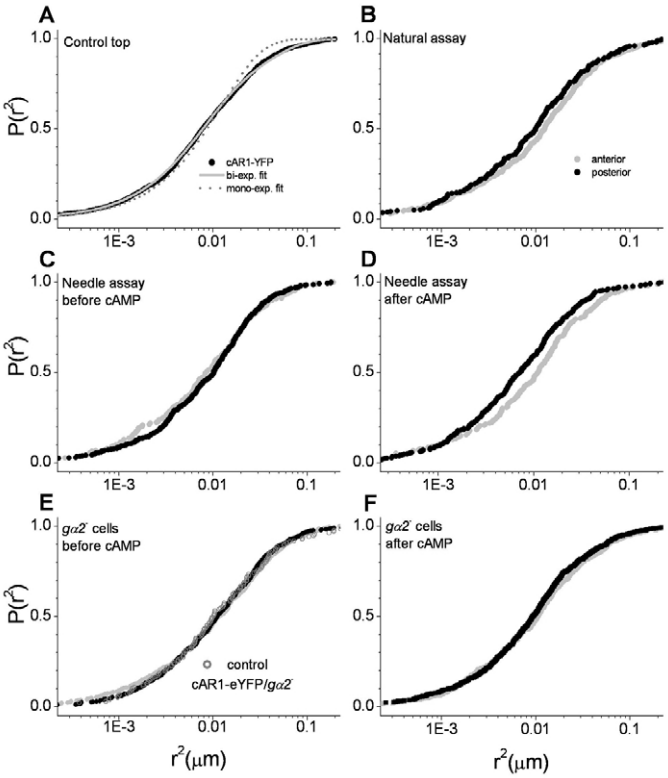


**Fig. 2.** Diffusion of cAR1-eYFP for resting cells and polarized cells. (A) Cumulative probability distribution of squared displacements, $P(r^2)$, of the trajectories ($n$=2060) of cAR1-eYFP from the top membrane of resting cells (control, black circles), recorded with $t_{lag}$=44 mseconds lag time between subsequent images. Data were fitted to a two-component model (equation 1) (grey curve), resulting in a fraction of immobile receptors, a fraction of mobile receptors and the mean squared displacement (MSD) of mobile receptors. The diffusion constant, D, was determined from: $MSD=4Dt_{lag}+4\sigma^2=0.034\pm0.003$ μm² with a lateral accuracy σ=40 nm given by our experimental conditions. 38±4% (mean±s.e.m.) of the receptors were mobile, characterized by a diffusion constant D=0.17±0.02 μm²/s. Fit to a one-component model (broken line, grey) did clearly fail to describe the data. (B) Cumulative probability distribution of squared displacements of cAR1-eYFP from the top membrane of the anterior (grey circles, $n$=526), and posterior (black circles, $n$=282) of polarized *car1*⁻ cells in the natural assay. By fitting both $P(r^2)$ with the two-population model, 44±4% and 39±4% of the anterior and posterior receptors, respectively, were found to be mobile, which was significantly different according to a two-sample Kolmogorov-Smirnov test (KS-test) with an acceptance level of 93.5%. (C) Cumulative probability distribution of squared displacements of cAR1-eYFP from the top membrane of the anterior ($n$=193) and posterior ($n$=368) sides of gradient-sensing competent *car1*⁻ cells in relation to the position of the needle before the cAMP gradient was initiated. The mobile fraction of the receptors was not different between anterior and posterior, and was equal to the control, as tested with a KS-test with an acceptance level of 93.5%. (D) Cumulative probability distribution of squared displacements of cAR1-eYFP from the top membrane of the anterior ($n$=225) and posterior ($n$=367) of gradient-sensing *car1*⁻ cells. After the needle filled with 10 μM cAMP was placed, 54±5% and 31±3% of the receptors were found to be mobile, respectively. (E) Cumulative probability distribution of squared displacements of cAR1-eYFP from the top membrane of the anterior ($n$=404) and posterior ($n$=509) of gradient-sensing *gα2*⁻ cells before the needle with cAMP was placed. 57±6% and 59±6% of the receptors were found to be mobile, respectively. (F) Cumulative probability distribution of squared displacements of cAR1-eYFP from the top membrane of the anterior ($n$=531) and posterior ($n$=687) of gradient-sensing *gα2*⁻ cells after the needle filled with 10 μM cAMP was placed. 51±5% and 49±5% of the anterior and posterior receptors, respectively, were found to be mobile.

with an acceptance level of 93.5% to the distributions. The KS-test applied to the data in Fig. 2B showed that receptors at the anterior had a higher mobility compared with receptors at the posterior of chemotaxing cells. Receptors at the posterior of chemotaxing cells were characterized by a mobility that was identical to that of the control (Fig. 2A).

More pronounced differences were obtained for polarized cells that sensed a gradient in a chemotaxis needle assay. The opening (radius 0.25 μm) of a micropipette filled with 10 μM cAMP was placed at a distance of 75 μm from the cells. This experimental arrangement created a shallow gradient of 0.4 nM/μm. The anterior and the posterior regions of the cell were defined as the regions closest or farthest away from the position of the needle, respectively. Immediately before applying cAMP, polarized cells were randomly oriented with respect to the position of the needle, which led to an average receptor mobility irrespective of its position on the cell (Fig. 2C) that was equal to that of the control (Fig. 2A). Hence, as predicted for randomly oriented cells, receptor mobility was uniform in the ensemble average. After the cells sensed a gradient of cAMP (30-60 seconds after cAMP application) a difference in mobility was clearly observed (Fig. 2D): receptors at the leading edge had a higher mobility compared with those at the posterior, with the latter being indistinguishable from the control (Fig. 2A). In order to confirm those results obtained by the needle assay, cells were exposed to a global cAMP level of 1 mM for less than 5 minutes. Receptor mobility on the whole cell was found to be indistinguishable from that found at the front of gradient-sensing cells in the needle assay (see supplementary material Fig. S1E).

For a better understanding what this higher mobility entailed, a quantitative description of the data was obtained by global analysis of the squared displacement distributions (Fig. 2). The cumulative probability distributions of squared displacements, $P(r^2)$, as shown in Fig. 2, were fitted to a two-population model, reflecting a mobile receptor fraction and an immobile receptor fraction (Schutz et al., 1997):

$$P(r^2) = 1 - \alpha \exp(-r^2/MSD) - (1-\alpha)\exp(-r^2/4\sigma^2) \quad (1)$$

Equation 1 leads to a characteristic mean squared displacement, MSD, and a fraction of mobile receptors, α. In our experiments, the lateral accuracy was found to be σ=40 nm. Assuming that mobile receptors were characterized by one characteristic MSD, all data (Fig. 2) were fitted simultaneously, yielding a fraction α (Fig. 3) for each data set and the corresponding characteristic MSD. The receptors were characterized by MSD=0.034 μm², which, using the delay between two observations of $t_{lag}$=44 mseconds, translates into a diffusion constant of $D=(MSD-4\sigma^2)/4t_{lag}=0.17\pm0.02$ μm²/second. In the control, 38% of the receptors were mobile (Fig. 2A), whereas 44% and 39% were mobile in the natural assay at the anterior and the posterior side of the cell, respectively (Fig. 2B). For the needle assay mobile fractions of 54% and 31% were determined at the anterior and the posterior of the cells, respectively (Fig. 2D). Hence, receptor stimulation by cAMP increases the fraction of mobile receptors at the anterior of the cell by a factor of 54/31 (i.e. 1.7) when compared with receptors at the posterior. Furthermore, the shift in mobile fraction observed in the natural assay (Fig. 2B) was reduced compared with the shift in the needle assay (Fig. 2D). This difference is readily explained by taking into account that, in the natural assay, cAMP is produced in waves within which the local gradient exists for only part (50%) of the cycle. Consequently, the difference in mobile fraction observed in the needle assay (54% versus 31%) is reduced by half for the natural assay which fully accounts for our findings (Fig. 2B).

The change in mobile fraction was not due to a change in membrane viscosity, as the mobile fraction of an inert membrane

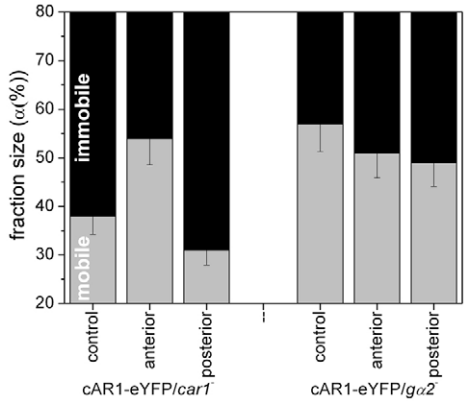


**Fig. 3.** Mobile fraction. Fraction of the mobile receptors (grey) characterized by a diffusion constant D=0.17±0.02 μm$^2$/s and that of immobile receptors (black). The fractions were compared in resting cells (control), and in anterior and posterior of gradient-sensing polarized cells. The polarized cells were measured either in the chemotaxis needle assay.

marker (individual concanavilin A conjugated with Alexa647 molecules were followed) was position independent even for polarized cells (see supplementary material Fig. S1). The distributions of receptors in the posterior for both the natural and the needle assay were, within experimental error, indistinguishable from the distribution in control cells. This indicates that only receptors at the anterior exhibit a specific, spatially restricted response to the chemoattractant. The latter finding is taken here as a first evidence that the chemoattractant receptor shows a spatially restricted response upon cAMP-induced activation in chemotaxis.

The issue of whether the difference in mobile fraction between the anterior and the posterior of gradient-sensing *D. discoideum* cells was caused by a conformational change of the receptor owing to its phosphorylation state, or by an altered interaction between the cAR1 receptor and its associated G-protein, was addressed by comparative studies with mutant cell lines. We analyzed a phosphorylation deficient mutant expressing a cAR1 receptor in which the four serine clusters in the C-terminal tail were substituted (cm1234-eYFP) (Kim et al., 1997). cm1234-eYFP/*car1*$^-$ cells were found to be defective in propagation of the cAMP wave (Kim et al., 1997), leading to very small aggregation centres during development. Therefore, cells expressing cm1234-eYFP were measured very close to the aggregation centre, a situation reflecting that of the needle assay. For cm1234-eYFP, the fraction of mobile receptors at the anterior exceeded that at the posterior by a factor of 1.7 (72% versus 43%, see supplementary material Fig. S1). This ratio was similar to that found for cAR1-eYFP during the needle assay (Fig. 2D). These results demonstrate that the pronounced shift of receptor mobile fraction was independent of the phosphorylation state of the receptor.

By comparison, experiments on cAR1-eYFP expressed in a mutant cell line lacking the Gα2 subunit cAR1-eYFP/*gα2*$^-$ produce significantly different results. It should be noted that, although cAR1-eYFP/*gα2*$^-$ cells were unable to aggregate, cAMP gradient sensing by the receptor was not impaired given that cAR1-eYFP was constitutively expressed and enabled its activation (or binding) by cAMP. The effect of the Gα2 protein on the mobility of the cAR1-eYFP receptor was studied by comparing cAR1-eYFP mobility in control cAR1-eYFP/*gα2*$^-$ and in control cAR1-eYFP/*car1*$^-$ cells (compare control in Fig. 2A,E). The distributions of cAR1-eYFP squared displacements were significantly different for the two cells lines. No difference in cAR1-eYFP mobility between control and starved cAR1-eYFP/*gα2*$^-$ cells was observed independently of the presence of a cAMP gradient (Fig. 2E,F). The mobile receptor fraction in *gα2*$^-$ cells (51%, Fig. 3) was, for all conditions, comparable with that at the anterior of gradient sensing *car1*$^-$ cells, and independent of receptor localization. These findings together suggest that the population of immobile receptors in cAR1-eYFP/*car1*$^-$ cells that became mobile upon cAMP addition would represent receptors that became uncoupled from their associated Gα2 protein upon cAMP stimulation.

As binding of the receptor to the GDP-bound inactive Gα2$^{GDP}$/βγ is expected to result in only a minor decrease in receptor diffusion constant, given the logarithmic dependence of D on receptor size (Saffman and Delbruck, 1975), pure binding can not account for the dramatic slowdown observed. One likely explanation follows from the postulated idea that G proteins interact with the cytoskeleton meshwork via protein complexes on microtubule plus ends (Rogers et al., 2004; Hampoelz and Knoblich, 2004). The microtubule plus-end complex seems to be required for the capture of microtubule tips at cortical sites by mediating interactions of microtubule tips with cortical actin, as well as with membrane proteins; this process plays a major role in nuclear migration, spindle formation and directed cell movement (Hestermann et al., 2002; Siegrist and Doe, 2007). As the mechanisms underlying chemotaxis are highly conserved and various proteins of this complex have been identified in *D. discoideum* (Hestermann et al., 2002), we propose a similar linkage to explain our results in *D. discoideum*. A stable anchoring of the receptor via Gα2 to the cytoskeleton would lead to a larger fraction of immobile receptors. To test this hypothesis, we applied Latrunculin B to control cells, which confirmed our prediction. The mobile fraction increased from 38% to 58% (see supplementary material Fig. S1). The change in receptor mobile fraction had already occurred in control cells, which confirmed that ligand-induced actin polymerization also did not play any role in those observations, given that *Gα2*$^-$ cells are deficient in a chemoattractant-induced response (Kumagai et al., 1989).

Although the results reported above were compelling evidence for the hypothesis that Gα2, via cytoskeleton anchoring, controls the mobility of cAR1, one might argue that the change in mobile fraction was a secondary effect caused by downstream signalling components. The latter must be absent in *Gα2*$^-$ cells in which the downstream signalling is impaired. The lack of change in membrane viscosity upon stimulation (supplementary material Fig. S1), however, suggests that this is not the case. In addition, the mobility of cAR1-eYFP in a *pi3k*$^{-/-}$ background displayed the same change in mobile fraction upon stimulation when compared with the *wt*-cells (supplementary material Fig. S1). Furthermore, wild-type cells treated with the PI3K inhibitor LY294002 (Loovers et al., 2006) and a *pi3k*$^{5-}$, *pten*$^-$ mutant in which all PI3K and PTEN genes were knocked out (Hoeller and Kay, 2007) exhibit a phenotype in terms of chemoattractant sensing similar to that of the *pi3k*$^{-/-}$ mutant. Together, this suggests that the cause of the shift in mobile fraction observed of cAR1 is located upstream of PI3K.

## Discussion

In conclusion, our data suggest that the immobile fraction of receptors that become mobile upon stimulation reflects inactive receptors bound via Gα2$^{GDP}$ to cytoskeletal elements. In addition to this cAMP-responsive fraction, a second pool of immobile receptors that did not change their mobility upon stimulation was

observed for all cells. This pool of cAMP-irresponsive receptors might be differently coupled to cellular structures that are static during the measurement (10-100 ms). Similarly, the mobile population found in control cells might indicate that there is a basal level of receptor activity. A more likely explanation though is that not all of cAR1 is precoupled to the G protein, a notion that has been suggested in several studies of mammalian GPCRs (Hein et al., 2005; Azpiazu and Gautam, 2004; Chisari et al., 2007). With reference to the results obtained on the cm1234-eYFP mutant, it should be noted that phosphorylation of the receptor is independent of G-protein signalling, as G-protein re-association still occurred on phosphorylated receptors (Janetopoulos et al., 2001).

Fig. 4A summarizes our findings and incorporates them into a model that relates a biological function for the increased mobile fraction of cAR1. Receptors normally reside in an inactive $G\alpha 2\beta\gamma^{GDP}$ precoupled state and are immobile. Upon receptor activation, $G\alpha 2\beta\gamma^{GDP}$ is processed into $G\alpha 2^{GTP}$ and dissociates both from the receptor and from its Gβγ partners. In turn, the receptor is decoupled from structural elements and becomes mobile. Accordingly, it is able to activate other $G\alpha 2\beta\gamma^{GDP}$ hetero-trimers. In the last step, receptor reassociation with the G protein is paralleled by anchorage to structural elements and receptor immobilization.

Inherent to most models describing directional sensing (Charest and Firtel, 2006; Janetopoulos et al., 2004; Postma and Van Haastert, 2001) is an initial linear amplification step for which our findings possibly yield a molecular interpretation. Assuming that G-protein activation is solely a diffusion-limited process, the higher mobile fraction of receptors at the anterior will increase the rate of activation of G proteins in proportion to the diffusion constant. Taking the off-rate of cAMP from the receptor, $k_{off}$=0.39/second (Ueda et al., 2001), as a typical timescale, the associated distance of an activated receptor movement becomes $\sqrt{4D/k_{off}}$=1.40 μm which is far enough to activate additional G proteins at an estimated concentration of ~$10^2$/μm$^2$. The amplification step proposed here, one receptor activating multiple G-proteins, will lead to a higher local G-protein excitation at the anterior, as a result of the difference in receptor occupancy. We suggest here that this initial linear amplification step might be crucial for crossing a threshold, as set by constitutive signal inhibition (e.g. by PTEN), and for subsequent signal propagation. Higher local G-protein excitation at the anterior has been monitored previously by fluorescence resonance energy

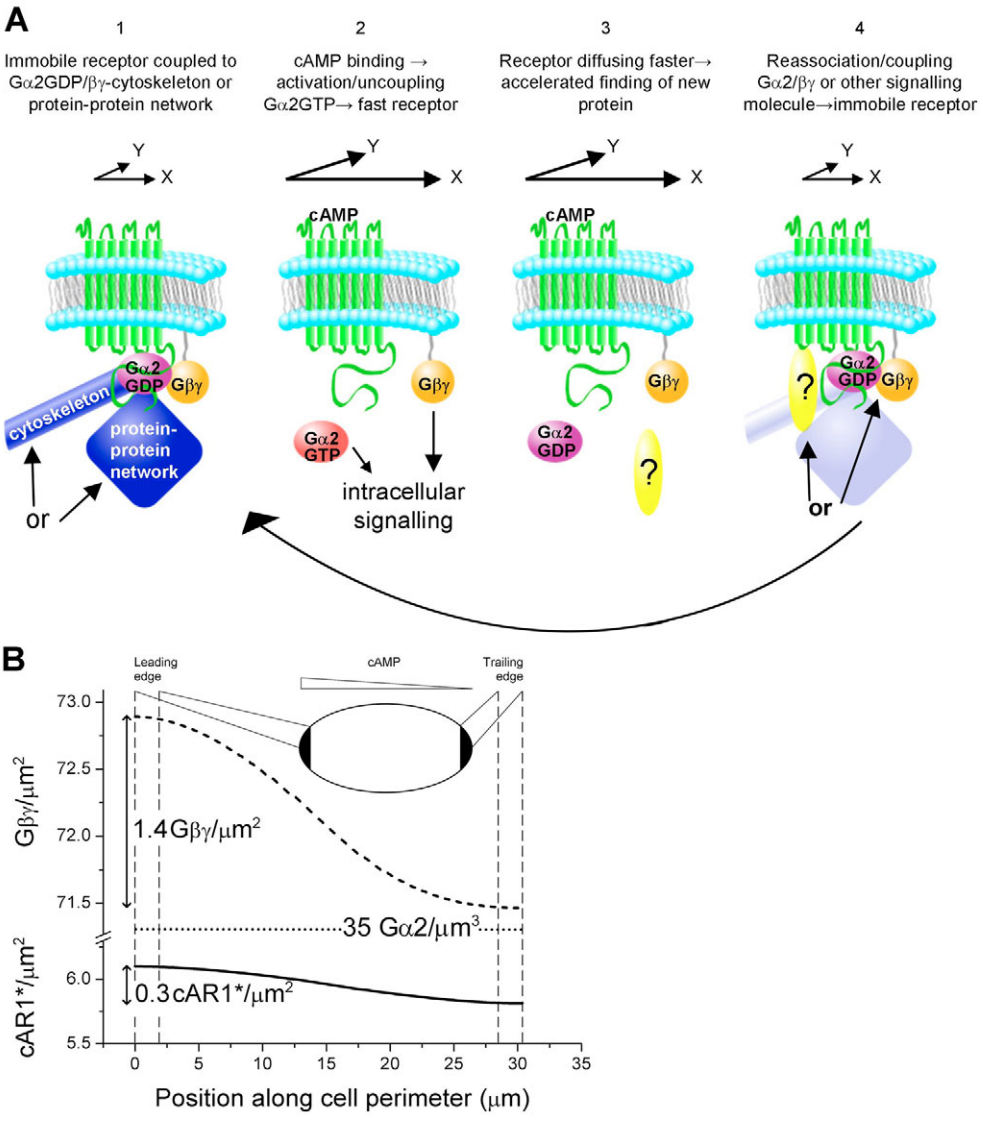


**Fig. 4.** Model describing accelerated signalling at the leading edge. (A) In resting cells, we found two receptor populations: immobile and mobile receptors. A fraction of the immobile receptors is coupled to $G\alpha 2^{GDP}/G\beta\gamma$, which, in turn, is coupled to protein-protein networks and/or the cytoskeleton which inhibits diffusion (1). This fraction of immobile receptors becomes mobile by uncoupling of $G\alpha 2^{GTP}$ upon cAMP activation. Free $G\alpha 2^{GTP}$ and free Gβγ subunits activate intracellular signalling (2). The mobile receptors have the ability to further activate other $G\alpha 2^{GDP}/G\beta\gamma$ complexes in a diffusion-limited process (3). In a final step, re-association of the receptor with $G\alpha 2^{GDP}/G\beta\gamma$ and corresponding loss of cAMP immobilizes the receptor again (4). (B) An ellipsoidal cell is exposed to a gradient of 0.4 nM/μm cAMP. The concentration at the leading edge is 66 nM and that at the trailing edge 58 nM. The density of active cAR1 receptor (cAR1*) is plotted versus the position along the cell membrane. At the leading edge the density of active cAR1 is higher by a factor of 1.05 when compared with the density at the trailing edge (6.1 molecules/μm$^2$ versus 5.8 molecules/μm$^2$) following the cAMP gradient. The density of activated Gβγ at the leading edge was 73.0 molecules/μm$^2$, whereas that at the trailing edge was 71.4 molecules/μm$^2$. Hence, diffusion leads to a linear amplification of the gradient by a factor of 5.

transfer between Gα and Gβγ, but has been interpreted only in terms of receptor occupancy (Xu et al., 2005). If we further assume that the probability of the loss of cAMP from the receptor is related to the process of G-protein activation, i.e. collision, the above mechanism also explains the increased cAMP off-rate at the anterior of the cell (Ueda et al., 2001).

To test whether the measured values would lead to the proposed linear amplification, a finite element model of the cellular processes was implemented in VCell (see Materials and Methods). In the model, the receptor cAR1 was activated upon cAMP binding, resulting in an activated cAR1 (hereafter referred to as cAR1*). cAR1* in turn was allowed to catalyze the dissociation of the Gα2βγ heterotrimer into membrane-localized Gβγ and cytosolic Gα2 (see supplementary material Fig. S2). Using estimates for concentrations known (see supplementary material Table S1) and for rate constants (see supplementary material Table S2), the effect of diffusion on the ability of cAR1* to activate multiple G proteins was investigated. As predicted, receptors activated multiple G proteins in the case of mobile receptors. At equilibrium conditions, 240 active cAR1* receptors at the leading edge activated 2866 Gβγ-proteins, whereas at the trailing edge, 228 cAR1* molecules activated 2802 Gβγ-proteins (Fig. 4B). The gradient is thus translated from an anterior/posterior difference of ten activated cAR1* receptors to a difference of 64 activated Gβγ-proteins, a fivefold linear amplification of the difference signal. It should be noted that signal amplification prevailed even at a ten times lower cAMP gradient, for which an even larger linear signal amplification of 20 was found (not shown). Next to a significant amplification of the primary signal, the finite-element model clearly confirms that gradient sensing must be transduced via activated membrane-bound Gβγ. The high mobility of cytosolic Gα2 completely washes out any external gradient, a result that had been predicted by the so-called depletion model (Postma and Van Haastert, 2001).

In this study, we found a cAMP-induced increase in the amount of mobile cAR1 receptors at the leading edge of cells. We showed that the acquired mobility of cAR1 allows for the receptor to activate multiple G proteins in the membrane and the simple model introduced above shows a fundamental type of physical amplification process that occurs at the very beginning of a signalling pathway. The experimental results, however, yielded a difference in mobile receptors between anterior and posterior of a factor of ~1.7. Hence, in order to explain our experimental data fully, a non-linear process will have to be incorporated into an improved model. The latter might include, for example, a cAR1*-induced cAR1 activation, the potential role of which must be verified in future experiments. Another explanation could be that the initial amplification, as predicted by the linear model, is enforced by an unknown feedback mechanism that affects the G protein coupling to the receptor. A recent study in mammalian cells revealed a shuttling of the G protein subunits between the cytoplasm and the membrane. It is therefore very feasible that the dynamic process of G protein coupling to the G protein-coupled receptor could be affected by downstream signalling components. This is currently tested in *D. discoideum*. Certainly, in order to understand the whole process of spatially restricted responses and chemosensing, including known feedback mechanisms and downstream processes (Charest and Firtel, 2006), more complex models, such as the local-excitation global-inhibition [LEGI (Ma et al., 2004)] or the diffusion-translocation model (Postma and Van Haastert, 2001), will have to be incorporated. These models do, however, benefit from the primary linear amplification our model predicts: the primary amplification may act as the compass of the cell during directional sensing. Considering the highly conserved nature of G-protein coupled receptor signalling in eukaryotes, our model might have even broader applications for other G-protein-coupled receptor signalling pathways.

## Materials and Methods

### cAR1-eYFP fusion protein

To create C-terminal YFP-tagged cAR1, eYFP DNA was created by PCR. The N-terminal primer CGGCTAGCATGGTGAGCAAGGGCGAGGAG contained an *Xba*I1 site at 5′ end, followed by the N-terminal residues of eYFP. The C-terminal primer GCTCTAGACTTGTACAGCTCGTCCATGCC contained the last seven residues of eYFP, followed by a *Nhe*I site. peYFP (from CLONTECH) was used as the template. The PCR products were double digested with *Xba*I1 and *Nhe*I, and then cloned into the *Nhe*I site of the *D. discoideum* cAR1 expression plasmid (Parent et al., 1998). The DNA was purified and transformed into JB4 cells (*car1*$^{-}$) or *Gα2*$^{-}$ cells by electroporation (Zigmond et al., 1981). Clones were grown up in a Petri dish in HL5-medium containing 10 μg/ml G418. Cells were cultured in six-well plates in axenic medium with addition of 100 μg/ml ampicillin and 100 μg/ml mixture of penicillin and streptomycin (1:1) at 22°C.

The expression level of the cAR1-eYFP in *car1*$^{-}$ cells was calculated in the following manner. The fluorescence of the cells at the membrane before measurement was on average five-times higher than the fluorescence expected for a single molecule (1000 cnts/3 mseconds versus 185 cnts/3 mseconds) based on the fluorescence of single YFP molecules in an artificial lipid membrane (Harms et al., 2001). Thus, there were on average five receptors within each diffraction-limited area [$s=\pi r^2=0.03$ μm$^2$, with $2r=1.22\times\lambda/(2NA)$ (i.e. 220 nm), for a wavelength (λ) of 514 nm]. For the whole cell, the surface of the membrane was $S=4\pi R^2=314$ μm$^2$, where R=5 μm is the typical radius of the cell. This leads to a total number of receptors $n=5$ S/s$=4\times10^4$, which is comparable with the expression level of endogenous receptors in wild-type cells (Johnson et al., 1991; Van Haastert, 1987).

### Developmental test in *car1*$^{-}$ expressing cAR1-eYFP

Transformants were plated on non-nutrient plates at a concentration of $10^7$ cells/ml. Development was monitored for the next 30 hours with a confocal microscope (Leica MZFLIII).

### Immunoblotting

*car1*$^{-}$ and cAR1-eYFP/*car1*$^{-}$ cells were solubilized with SDS-sample buffer and resolved by SDS-PAGE on 10% gels along with a set of protein MW standards. cAR1-eYFP was detected by immunoblot with anti-GFP antibody. Free YFP was also run on the gel and immunoblotted.

### Cell preparation and measurement

Control cells were transferred to phosphate buffer (0.534 g $Na_2HPO_4$, 0.952 g $KH_2PO_4$ in 1 litre of $H_2O$, set pH to 6.5) after one night in low-fluorescence medium (Liu et al., 2002) and measured after 1 hour. This procedure was required to lower the intrinsic autofluorescence as described by de Keijzer et al. (de Keijzer et al., 2007). Low-fluorescence medium contains few nutrients and therefore control cells are not vegetative, but their state is estimated to be comparable with 2-3 hours of starvation. These cells were not able to migrate towards the cAMP source in the needle assay. For the experiments with the natural assay, the cells were starved at a concentration of $10^5$ cells/ml in phosphate buffer for 20 hours at 16°C. For the chemotaxis needle assay, the cells were maintained overnight in low-fluorescence medium and starved for 6-8 hours in phosphate buffer at 22°C. Before measuring, the cells were tested to be aggregation competent. All measurements were performed in two-well, chambered coverglasses (1.5 Borosilicate Sterile, Lab Tek II).

The cells were placed in a distance of 75 μm from the opening (r=0.25 μm) of a pipette filled with 10 μM of cAMP. The internal pressure in the pipette was set to 40 kPa by means of a FemtoJet injector (Eppendorf). This setup created a stable, shallow gradient of 0.4 nM/μm cAMP over the cell. Before applying cAMP, randomly oriented polarized cells were measured in a region that was either facing or opposite of the position of the needle. After applying cAMP, the cells, oriented in a front-back alignment towards the position of the needle, were measured within 1 minute, taking time to focus on the cell and perform single molecule measurements. At least 25 cells were measured for every condition.

### Labelling membrane with marker

Concanavalin A Alexa647 conjugate (Invitrogen) was used as a marker to label the plasma membrane. Concanavalin A (ConA) selectively binds to α-mannopyranosyl and α-glucopyranosyl residues. Cells where incubated for 10-15 minutes in 1 ml of 80 ng/ml ConA in PB. The excess marker was removed by washing the cells three times with PB before measuring. The low concentration in combination with the short incubation time prevented formation of ConA clustering, and allowed us to follow individual ConA bound to the plasma membrane.

### Single-molecule microscopy

The experimental setup for single-molecule imaging has been described in detail previously (Schmidt et al., 1996). The samples were mounted onto an inverted microscope (Axiovert100, Zeiss) equipped with a 100× objective (NA=1.4, Zeiss). The region-of-interest was set to 50×50 pixels. The apparent pixel-size was 220 nm. Measurements were performed by illumination of the samples for 5 ms at 514 nm (Argon-ion laser, Spectra Physics) at an intensity of 2 kW/cm$^2$. The cells were photobleached for a period of 2.5-5 seconds before a typically sequence of 100 images with timelag of 44 ms were taken. It should be noted that this procedure did not harm the cells, and that cells chemotax normally after the procedure. Use of appropriate filter combinations (DCLP 530, HQ570/80; Cy3/Cy5, Chroma Technology, and OG 530, Schott) permitted the detection of the fluorescence signal on a liquid nitrogen-cooled CCD-camera (Princeton Instruments). The total detection efficiency of the experimental setup was 8%. This setup allows imaging of individual fluorophores within a time-frame of a few milliseconds at a signal-to-background-noise ratio of 30. In these conditions and for millisecond integration periods, the auto-fluorescent proteins have photon emission rates of ~3000 photons/msecond, saturation intensities from 6-50 kW/cm$^2$, and photo-bleaching yields from $10^{-4}$ to $10^{-5}$. It was reported earlier that eYFP is superior compared with all the fluorescent proteins for single-molecule studies in vivo using wide-field microscopy (Harms et al., 2001).

### Fitting algorithm with background subtraction

Each image of an image stack contained in addition to the fluorescence signals from individual YFP molecules autofluorescence from the cell. In order to correct for autofluorescence, an algorithm was developed that subtracted a sliding weighted-mean image from each image of the sequence. The weights were Gaussian distributed with a width of 40 images. Using this algorithm, any slow-moving stable signal, i.e. a bright vesicle, was effectively removed, whereas fast-moving or fast bleaching signals, like individual molecules, prevailed. The algorithm was validated by simulation, containing Brownian trajectories, the corresponding fluorescent molecules, autofluorescence computed from a typical file and additional camera noise.

### Fitting the cumulative possibility distributions of the squared displacements

The trajectories of individual molecules were constructed and analyzed as described previously (Lommerse et al., 2005). To compensate for the limited length of individual trajectories owing to photobleaching of eYFP, multiple data sets, each consisting of hundreds of trajectories from >25 cells per experimental condition, were analyzed. The trajectories were analyzed in terms of squared displacement ($r^2$), and fitted by models describing the lateral diffusion of Brownian particles in a medium characterized by a diffusion coefficient D using the cumulative distribution function of the squared displacements, $r^2$ (Anderson et al., 1992; Almeida and Vaz, 1995). After fitting the data with a model describing one population (Fig. 2A) we chose a model in which two populations of receptors, mobile receptors with diffusion constant, D, and immobile receptors were assumed (Schutz et al., 1997). We made the assumption that the diffusion constant of the receptor was not changed with genetic background. This assumption is substantiated by our finding that the fluidity of the membrane was the same for the anterior and posterior of the cell. The squared displacements of all measurements (all datasets) were analyzed simultaneously, yielding the diffusion constant of a mobile receptor of D=0.17±0.02 μm$^2$/second. Our global-fit approach was further controlled by extraction of a diffusion constant from of each data set independently. Within the accuracy range all diffusion constants were found to be the same, indicating that our assumption was appropriate. The effect of cell motility (v<10 μm/minute) could be neglected because of the short time lag ($t_{lag}$=44 mseconds) in the current study leading to an positional averaging of $(v\times t_{lag})^2<5.4\times10^{-5}$ μm$^2$, much smaller than the positional accuracy of $4\sigma^2=6.4\times10^{-3}$ μm$^2$.

### Finite element model

A finite element model was implemented using the VCell modelling environment (Loew and Schaff, 2001). The model included extracellular cAMP and membrane localized cAR1, Gα2βγ, Gβγ and cytosolic Gα2. The cAR1 receptor was activated upon cAMP binding, resulting in cAR1*. cAR1* in turn was allowed to catalyze the dissociation of the Gα2βγ heterotrimer into membrane localized Gβγ and cytosolic $G\alpha_2$ (see supplementary material Fig. S2). Using the parameters listed in Tables S1 and S2, we investigated the effect of diffusion on the ability of cAR1* to activate the G protein.

The cell was modelled as an ellipsoid, the long axis of which was set to 20 μm and the other axes had a length of 10 μm. The leading and trailing edge were defined as the surfaces at the anterior and posterior for which the radius was half the full radius of the cell. The surface area of the leading and trailing edge thus were both 40 μm$^2$.

The concentration of cAMP was based on the concentration the cells experience when they are 75 μm away from a pipette filled with 10 μM of cAMP and an opening of 0.25 μm. The mid-concentration was 62 nM and the gradient 0.4 nM/μm. All results where obtained at equilibrium conditions. The number of cAR1 receptors was estimated to be $4\times10^4$/cell (Johnson et al., 1991; Van Haastert, 1987), which translates to a density of ~25 cAR1/μm$^2$ at the membrane, given the number of receptors that were able to respond in our experiment (20%). The number of Gα2βγ was estimated to be $7.5\times10^4$/cell (Snaar-Jagalska et al., 1988), leading to a density of 240 Gα2βγ/μm$^2$ at the membrane.

The diffusion constant of inactive cAR1 and of the active cAR1* were based on our measurements. The diffusion constant of the Gα2βγ was set to the error in positional accuracy as we assumed Gα2βγ to be bound to intracellular structures. The diffusion constant of Gβγ was based on that reported for the hRas-anchor, 0.5 μm$^2$/seconds (Lommerse et al., 2005), and that of Gα2 was based on that of free GFP in the cytosol of *D. discoideum*, 24 μm$^2$/seconds (Ruchira et al., 2004).

Given the reverse rate constant for cAR1 activation Kr_1=0.39/second (Ueda et al., 2001), and the dissociation constant $K_D$=42 nM (Van Haastert and Kien, 1983) the primary reaction was characterized. The rates for both the cAR1*-catalyzed G-protein activation as well as that of the spontaneous G-protein inactivation were assumed to be diffusion limited (Berg, 1993) leading to Kf_2=0.66 μm$^2$/molecule/second, and Kr_2=100/μM/second, respectively.

We thank G. A. Blab for help with the data analysis, Yu Long (Devreotes laboratory) for the cAR1-eYFP construct, and T. Durston, P. M. Brakefield and P. N. Devreotes for comments on the manuscript. This work was supported by funds from the Dutch CW/NWO project 700-50-032, a Human Frontiers Science Program grant RGP66/2004 and the Dutch CYTTRON consortium sponsored by the ministry of economic affairs. A.S. was supported by a European Union fellowship (HPMF-CT-2001-01285).

## References

**Affolter, M. and Weijer, C. J.** (2005). Signaling to cytoskeletal dynamics during chemotaxis. *Dev. Cell* **9**, 19-34.

**Almeida, P. F. F. and Vaz, W. L. C.** (1995). Lateral diffusion in membranes. In *Handbook of Biological Physics* (ed. R. Lipowsky and E. Sackmann), pp. 305-357. Amsterdam: Elsevier/North Holland.

**Anderson, C. M., Georgiou, G. N., Morrison, I. E., Stevenson, G. V. and Cherry, R. J.** (1992). Tracking of cell surface receptors by fluorescence digital imaging microscopy using a charge-coupled device camera. Low-density lipoprotein and influenza virus receptor mobility at 4 degrees C. *J. Cell Sci.* **101**, 415-425.

**Azpiazu, I. and Gautam, N.** (2004). A fluorescence resonance energy transfer-based sensor indicates that receptor access to a G protein is unrestricted in a living mammalian cell. *J. Biol. Chem.* **279**, 27709-27718.

**Berg, H. C.** (1993). *Random Walks in Biology*. Princeton: Princeton University Press.

**Charest, P. G. and Firtel, R. A.** (2006). Feedback signaling controls leading-edge formation during chemotaxis. *Curr. Opin. Genet. Dev.* **16**, 339-347.

**Chen, L., Iijima, M., Tang, M., Landree, M. A., Huang, Y. E., Xiong, Y., Iglesias, P. A. and Devreotes, P. N.** (2007). PLA2 and PI3K/PTEN pathways act in parallel to mediate chemotaxis. *Dev. Cell* **12**, 603-614.

**Chisari, M., Saini, D. K., Kalyanaraman, V. and Gautam, N.** (2007). Shuttling of G protein subunits between the plasma membrane and intracellular membranes. *J. Biol. Chem.* **282**, 24092-24098.

**de Keijzer, S., Snaar-Jagalska, B. E., Spaink, H. P. and Schmidt, T.** (2008). Single-molecule imaging of cellular reactions in live cells. In *Single Molecules in Nanotechnology* (ed. R. Rigler and H. Vogel), pp. 107-131. Heidelberg: Springer.

**Devreotes, P. N.** (1994). G protein-linked signaling pathways control the developmental program of Dictyostelium. *Neuron* **12**, 235-241.

**Franca-Koh, J., Kamimura, Y. and Devreotes, P.** (2006). Navigating signaling networks: chemotaxis in Dictyostelium discoideum. *Curr. Opin. Genet. Dev.* **16**, 333-338.

**Hampoelz, B. and Knoblich, J. A.** (2004). Heterotrimeric G proteins: new tricks for an old dog. *Cell* **119**, 453-456.

**Harms, G. S., Cognet, L., Lommerse, P. H., Blab, G. A. and Schmidt, T.** (2001). Autofluorescent proteins in single-molecule research: applications to live cell imaging microscopy. *Biophys. J.* **80**, 2396-2408.

**Hein, P., Frank, M., Hoffmann, C., Lohse, M. J. and Bunemann, M.** (2005). Dynamics of receptor/G protein coupling in living cells. *EMBO J.* **24**, 4106-4114.

**Hestermann, A., Rehberg, M. and Graf, R.** (2002). Centrosomal microtubule plus end tracking proteins and their role in Dictyostelium cell dynamics. *J. Muscle Res. Cell Motil.* **23**, 621-630.

**Hoeller, O. and Kay, R. R.** (2007). Chemotaxis in the absence of PIP3 gradients. *Curr. Biol.* **17**, 813-817.

**Janetopoulos, C., Jin, T. and Devreotes, P.** (2001). Receptor-mediated activation of heterotrimeric G-proteins in living cells. *Science* **291**, 2408-2411.

**Janetopoulos, C., Ma, L., Devreotes, P. N. and Iglesias, P. A.** (2004). The chemoattractant-induced PI(3,4,5)P-3 accumulation is regulated by a local excitation, global inhibition mechanism. *Mol. Biol. Cell* **15**, 402A.

**Jin, T., Zhang, N., Long, Y., Parent, C. A. and Devreotes, P. N.** (2000). Localization of the G protein betagamma complex in living cells during chemotaxis. *Science* **287**, 1034-1036.

**Johnson, R. L., Vaughan, R. A., Caterina, M. J., Van Haastert, P. J. and Devreotes, P. N.** (1991). Overexpression of the cAMP receptor 1 in growing Dictyostelium cells. *Biochemistry* **30**, 6982-6986.

**Kesbeke, F., Vanhaastert, P. J. M. and Schaap, P.** (1986). Cyclic-AMP relay and cyclic AMP-induced cyclic-GMP accumulation during development of Dictyostelium-discoideum. *FEMS Microbiol. Lett.* **34**, 85-89.

**Kim, J. Y., Soede, R. D., Schaap, P., Valkema, R., Borleis, J. A., Van Haastert, P. J., Devreotes, P. N. and Hereld, D.** (1997). Phosphorylation of chemoattractant receptors is not essential for chemotaxis or termination of G-protein-mediated responses. *J. Biol. Chem.* **272**, 27313-27318.

**Kumagai, A., Pupillo, M., Gundersen, R., Miakelye, R., Devreotes, P. N. and Firtel, R. A.** (1989). Regulation and function of G-alpha protein subunits in Dictyostelium. *Cell* **57**, 265-275.

**Liu, T., Mirschberger, C., Chooback, L., Arana, Q., Dal Sacco, Z., MacWilliams, H. and Clarke, M.** (2002). Altered expression of the 100 kDa subunit of the Dictyostelium vacuolar proton pump impairs enzyme assembly, endocytic function and cytosolic pH regulation. *J. Cell Sci.* **115**, 1907-1918.

**Loew, L. M. and Schaff, J. C.** (2001). The Virtual Cell: a software environment for computational cell biology. *Trends Biotechnol.* **19**, 401-406.

**Lommerse, P. H. M., Snaar-Jagaiska, B. E., Spaink, H. P. and Schmidt, T.** (2005). Single-molecule diffusion measurements of H-Ras at the plasma membrane of live cells reveal microdomain localization upon activation. *J. Cell Sci.* **118**, 1799-1809.

**Loovers, H. M., Postma, M., Keizer-Gunnink, I., Huang, Y. E., Devreotes, P. N. and Van Haastert, P. J.** (2006). Distinct roles of PI(3,4,5)P3 during chemoattractant signaling in Dictyostelium: a quantitative in vivo analysis by inhibition of PI3-kinase. *Mol. Biol. Cell* **17**, 1503-1513.

**Ma, L., Janetopoulos, C., Yang, L., Devreotes, P. N. and Iglesias, P. A.** (2004). Two complementary, local excitation, global inhibition mechanisms acting in parallel can explain the chemoattractant-induced regulation of PI(3,4,5)P-3 response in Dictyostelium cells. *Biophys. J.* **87**, 3764-3774.

**Parent, C. A., Blacklock, B. J., Froehlich, W. M., Murphy, D. B. and Devreotes, P. N.** (1998). G protein signaling events are activated at the leading edge of chemotactic cells. *Cell* **95**, 81-91.

**Postma, M. and Van Haastert, P. J. M.** (2001). A diffusion-translocation model for gradient sensing by chemotactic cells. *Biophys. J.* **81**, 1314-1323.

**Rogers, S. L., Wiedemann, U., Hacker, U., Turck, C. and Vale, R. D.** (2004). Drosophila RhoGEF2 associates with microtubule plus ends in an EB1-dependent manner. *Curr. Biol.* **14**, 1827-1833.

**Ruchira, Hink, M. A., Bosgraaf, L., van Haastert, P. J. and Visser, A. J.** (2004). Pleckstrin homology domain diffusion in Dictyostelium cytoplasm studied using fluorescence correlation spectroscopy. *J. Biol. Chem.* **279**, 10013-10019.

**Saffman, P. G. and Delbruck, M.** (1975). Brownian motion in biological membranes. *Proc. Natl. Acad. Sci. USA* **72**, 3111-3113.

**Schmidt, T., Schutz, G. J., Baumgartner, W., Gruber, H. J. and Schindler, H.** (1996). Imaging of single molecule diffusion. *Proc. Natl. Acad. Sci. USA* **93**, 2926-2929.

**Schutz, G. J., Schindler, H. and Schmidt, T.** (1997). Single-molecule microscopy on model membranes reveals anomalous diffusion. *Biophys. J.* **73**, 1073-1080.

**Siegrist, S. E. and Doe, C. Q.** (2007). Microtubule-induced cortical cell polarity. *Genes Dev.* **21**, 483-496.

**Snaar-Jagalska, B. E., De Wit, R. J. and Van Haastert, P. J.** (1988). Pertussis toxin inhibits cAMP surface receptor-stimulated binding of [35S]GTP gamma S to Dictyostelium discoideum membranes. *FEBS Lett.* **232**, 148-152.

**Takeda, K., Sasaki, A. T., Ha, H., Seung, H. A. and Firtel, R. A.** (2007). Role of phosphatidylinositol 3-kinases in chemotaxis in dictyostelium. *J. Biol. Chem.* **282**, 11874-11884.

**Ueda, M., Sako, Y., Tanaka, T., Devreotes, P. and Yanagida, T.** (2001). Single-molecule analysis of chemotactic signaling in Dictyostelium cells. *Science* **294**, 864-867.

**Van Haastert, P. J.** (1987). Down-regulation of cell surface cyclic AMP receptors and desensitization of cyclic AMP-stimulated adenylate cyclase by cyclic AMP in Dictyostelium discoideum. Kinetics and concentration dependence. *J. Biol. Chem.* **262**, 7700-7704.

**Van Haastert, P. J. and Kien, E.** (1983). Binding of cAMP derivatives to Dictyostelium discoideum cells. Activation mechanism of the cell surface cAMP receptor. *J. Biol. Chem.* **258**, 9636-9642.

**Weiner, O. D.** (2002). Regulation of cell polarity during eukaryotic chemotaxis: the chemotactic compass. *Curr. Opin. Cell Biol.* **14**, 196-202.

**Xiao, Z., Zhang, N., Murphy, D. B. and Devreotes, P. N.** (1997). Dynamic distribution of chemoattractant receptors in living cells during chemotaxis and persistent stimulation. *J. Cell Biol.* **139**, 365-374.

**Xu, X. H., Meier-Schellersheim, M., Jiao, X. M., Nelson, L. E. and Jin, T.** (2005). Quantitative imaging of single live cells reveals spatiotemporal dynamics of multistep signaling events of chemoattractant gradient sensing in Dictyostelium. *Mol. Biol. Cell* **16**, 676-688.

**Zigmond, S. H., Levitsky, H. I. and Kreel, B. J.** (1981). Cell polarity: an examination of its behavioral expression and its consequences for polymorphonuclear leukocyte chemotaxis. *J. Cell Biol.* **89**, 585-592.

Journal of Cell Science

**Table S1**: Parameters of the finite-element model

| parameter | description | location | initial condition | units | D ($\mu m^2$/seconds) |
|---|---|---|---|---|---|
| cAMP | fixed gradient of cAMP | extracellular | fixed | $\mu M$ | 0 (fixed) |
| cAR1 | inactive cAMP receptor | membrane | 10.0 | molecules/$\mu m^2$ | 0.04 |
| cAR1* | active cAMP receptor | membrane | 0 | molecules/$\mu m^2$ | 0.17 |
| $G\alpha_2\beta\gamma$ | inactive G-protein heterotrimer | membrane | 140 | molecules/$\mu m^2$ | 0.04 |
| $G\alpha_2$ | $G\alpha_2$ subunit | cytosol | 0 | $\mu M$ | 24 |
| $G\beta\gamma$ | $G\beta\gamma$ subunit | membrane | 0 | molecules/$\mu m^2$ | 0.5 |

**Table S2**: Rate constants for finite-element model

| *Reaction* | *Rate constants* |
|---|---|
| $cAMP + cAR1 \underset{Kr\_1}{\overset{Kf\_1}{\rightleftharpoons}} cAR1^*$ | Kf_1 = 9.3 / μM / seconds<br>Kr_1 = 0.39 / seconds |
| $G\alpha_2\beta\gamma \underset{Kr\_2}{\overset{Kf\_2 \times cAR1^*}{\rightleftharpoons}} G\alpha_2 + G\beta\gamma$ | Kf_2 = 0.7 $\mu m^2$ / molecule / seconds<br>Kr_2 = 100 / μM / seconds |